

Kinematic characterisation of hexapods for industry

Julien Blaise and Ilian Bonev

Automated Manufacturing Engineering, École de technologie supérieure, Montréal, Canada

Bruno Monsarrat

Aerospace Manufacturing Technology Centre, National Research Council Canada, Montréal, Canada

Sébastien Briot

IRCCyN, Nantes, France, and

Jason Michel Lambert and Claude Perron

Aerospace Manufacturing Technology Centre, National Research Council Canada,
Campus de l'Université de Montréal, Montréal, Canada

Abstract

Purpose – The purpose of this paper is to propose two simple tools for the kinematic characterization of hexapods. The paper also aims to share the experience of converting a popular commercial motion base (Stewart-Gough platform, hexapod) to an industrial robot for use in heavy duty aerospace manufacturing processes.

Design/methodology/approach – The complete workspace of a hexapod is a six-dimensional entity that is impossible to visualize. Thus, nearly all hexapod manufacturers simply state the extrema of each of the six dimensions, which is very misleading. As a compromise, a special 3D subset of the complete workspace is proposed, an approximation of which can be readily obtained using a computer-aided design (CAD)/computer-aided manufacturing (CAM) software suite, such as computer-aided 3D interactive application (CATIA). While calibration techniques for serial robots are readily available, there is still no generally agreed procedure for calibrating hexapods. The paper proposes a simple calibration method that relies on the use of a laser tracker and requires no programming at all. Instead, the design parameters of the hexapod are directly and individually measured and the few computations involved are performed in a CAD/CAM software such as CATIA.

Findings – The conventional octahedral hexapod design has a very limited workspace, though free of singularities. There are important deviations between the actual and the specified kinematic model in a commercial motion base.

Practical implications – A commercial motion base can be used as a precision positioning device with its controller retrofitted with state-of-the-art motion control technology with accurate workspace and geometric characteristics.

Originality/value – A novel geometric approach for obtaining meaningful measures of the workspace is proposed. A novel, systematic procedure for the calibration of a hexapod is outlined. Finally, experimental results are presented and discussed.

Keywords Calibration, Aerospace industry, Kinematics, Robotics

Paper type Research paper

1. Introduction

The Stewart-Gough platform, also called hexapod, is the best-known and most commonly used parallel robot in industry. Hexapods have been used for several decades (Bonev, 2003), mainly for motion simulation (e.g. flight simulators). This type of product is designed to displace a load as heavy as several tons, and is typically referred to as a motion base or motion platform.

In recent years, there has been a growing interest in the use of parallel robots in the aerospace sector for manufacturing aircraft structures. Their high stiffness, high accuracy and low inertia make them good candidates to replace the typical serial structure of CNC machines, resulting in increased throughput and flexibility, and reduced production costs (Sàenz *et al.*, 2002). Examples of hybrid structures incorporating a tool head with parallel kinematics are DS Technologie's ECOSPEED and ECOLINER (Hennes and Staimer, 2004) and Fatronik's SPACE 5H (Collado and

The current issue and full text archive of this journal is available at www.emeraldinsight.com/0143-991X.htm



Industrial Robot: An International Journal
37/1 (2010) 79–88
© Emerald Group Publishing Limited [ISSN 0143-991X]
[DOI 10.1108/01439911011009984]

The authors would like to thank François Ferland, Technical Officer within the AMTC automation and robotics group for his support during the controller retrofit stage of the project. The authors would also like to acknowledge the Montreal-based company THCE for the integration and programming of the Delta Tau motion controller.

Herranz, 2004) machining centres. They all rely on the same arrangement where the parallel module, positioning a high-speed milling head, is mounted on a translational 2 degrees of freedom (DOF) unit in order to be able to work on large-scale aeronautic components.

Another recent tendency in the aerospace sector is the use of dynamic modules with parallel kinematics in reconfigurable tooling to replace dedicated tooling and/or specialized equipment for the assembly of aircraft structures (Kihlman and Engström, 2002; Kihlman *et al.*, 2004). In such applications, an external serial robotic system is used to sequentially reconfigure a set of passive tooling modules, those with 6 DOFs consisting of standard hexapods.

In this context, the Aerospace Manufacturing Technology Centre (AMTC) of the National Research Council Canada (NRC) is involved in a research initiative to investigate the industrialization of hexapods in heavy duty aerospace manufacturing processes such as drilling and milling of aerospace materials. An application with current particular emphasis is the positioning of heavy aeronautic components with very high accuracy using an active dynamically reconfigurable tooling based on parallel kinematics. In each configuration of the tooling, precision machining operations can be applied to the structural component using an external serial robot.

There exist a few commercial hexapods aimed for precise positioning, such as the F-200i, manufactured by Fanuc, but their payload is less than a 100 kg, unlike the payload of commercially available motion bases. On the other hand, although it might seem simple to manufacture a hexapod, companies such as Moog FCS, the leading manufacturer of motion systems, have decades of experience building hundreds of such motion systems. Even, leading flight simulator manufacturers such as computer-aided engineering (CAE), no longer build their own motion bases but purchase them from Moog FCS. Since high-payload capability was one of the main requirements for AMTC researchers, it was decided to proceed with the procurement of a heavy payload commercial motion system rather than manufacture a hexapod from scratch. The system acquired by the AMTC (Figure 1), a Moog FCS 5000E motion base, is equipped with electric actuators and can carry a payload of 2,500 kg.

Although, the hexapod's electro-mechanical design makes it very suitable for aerospace manufacturing applications, its

Figure 1 The 5000E motion base located at the NRC AMTC



positioning precision and tracking performance as provided by the factory controller were far off from the tolerances required by aerospace manufacturing processes. Furthermore, as it was used primarily in playback mode, the user interface capabilities in terms of online monitoring and path planning were severely limited from a research and development standpoint. For these reasons, it was decided at the time of procurement to also retrofit the factory controller with a commercial-off-the-shelf high-performance control platform. The selected motion controller was one developed by Delta Tau Data Systems. It had been previously implemented successfully for the motion control of the ALIO Industries 3- and 6-DOF parallel kinematic robotic micromanipulators designed for nanometer precision applications (Hennessey, 2004).

Before integrating the advanced robot controller, however, the hexapod's geometry needed to be fully characterized. No need to mention that the otherwise very complex six-dimensional hexapod workspace was succinctly described by the manufacturer in a six rows by six columns table (as is the case with nearly all commercial parallel robots). Furthermore, proper kinematic calibration of the hexapod geometry was necessary for the sake of achieving better absolute accuracy.

This paper first presents an original algorithm for computing a meaningful measure of the workspace of a hexapod using CATIA. In the second part, a simple procedure for calibrating a hexapod using a laser tracker is proposed. While this procedure is very intuitive, it has never been described before in the literature. Finally, the architecture of the retrofitted controller incorporating the determined workspace characteristics and calibration data is presented in the last section.

2. A new workspace measure for 6-DOF parallel robots

It is well known that hexapods (and parallel robots in general) have very limited workspace. Hence, it is extremely important to make optimal use of this small workspace, which requires a good knowledge of it.

As the complete workspace of a hexapod is a highly coupled entity in a six-dimensional space for which no human representation exists, different types of subsets of the complete workspace are usually determined in the academic community. Hexapod manufacturers would, however, simply specify only the largest six one-dimensional subsets (e.g. from its home position, the hexapod can move up or down 25 cm, without changing the platform's orientation). This information is obviously extremely insufficient and misleading.

In the academic community, the most commonly determined subset of the complete workspace of parallel robots is the constant-orientation workspace, which is the 3D volume that can be attained by the mobile platform's centre while the mobile platform is kept at a constant orientation. Therefore, in order to get a good understanding of the hexapod's complete workspace, one might represent a series of constant-orientation workspaces for various orientations. While this would be largely better than what hexapod manufacturers specify, such a representation is still of little practical value.

Fortunately, in various applications the hexapod's capability to rotate its platform about the platform's z -axis (torsion) is

not needed (e.g. in five-axis machining) or can be compensated otherwise. A common way of dealing with this redundancy is to use optimization methods in order to come up with the best configuration, given some criteria. However, as shown in Bonev and Ryu (1999), if the torsion is kept at zero (i.e. the platform only tilts about its horizontal axis), then the range for the remaining DOF is largely increased. While zero is not always the torsion angle value that maximized the workspace of a hexapod, it is a very good approximation and calls for no extra computations.

Thus, we propose a new 3D workspace subset that we name maximum tilt workspace. This workspace measure is defined as the set of positions that the centre of the mobile platform can attain with any direction of its z-axis making a tilt angle limited by a given value.

Before detailing our algorithm, however, we will describe a not well-known set of three angles for representing orientation, which is the key for our algorithm.

2.1 Tilt and torsion angles

A peculiar three-angle orientation representation, later called tilt-and-torsion (T&T) angles, was proposed in Bonev and Ryu (1999), in conjunction with a new method for computing the orientation workspace of symmetric spatial parallel robots. It was shown that T&T angles take full advantage of a robot’s symmetry. These angles were also independently introduced in Huang et al. (1999) and Wang (1999). Later, it was found out that the angles had been proposed in Korein (1984) under the name halfplane-deviation-twist angles. Yet again in 1999, these angles were proposed independently in Crawford et al. (1999) as a new standard in modeling angular joint motion, and particularly that of the spinal column’s vertebra. These angles are also used for computer animation of articulated bodies, known as the swing-and-twist representation.

In Bonev et al. (2002), the advantages of T&T angles in the study of spatial parallel robots were further demonstrated. It was shown that there is a class of 3-DOF parallel robots that have always a zero torsion, that we now call zero-torsion parallel robots.

T&T angles are defined in two stages – a tilt and a torsion. This does not, however, mean that only two angles define the T&T angles but simply that the axis of tilt is variable and is defined by another angle. In the first stage, shown in Figure 2(a), the body frame is tilted about a horizontal axis, *a*, at an angle *θ*, referred to as the tilt. The axis *a* is defined by an angle *φ*, called the azimuth, which is the angle between the projection of the body *z*₀-axis onto

the fixed *xy*-plane and the fixed *x*-axis. In the second stage, shown in Figure 2(b), the body frame is rotated about the body *z*₀ axis at an angle *σ*, called the torsion.

For space limitations, we will omit the details of the derivation process, and write directly the resulting rotation matrix of T&T angles, which is:

$$R(\phi, \theta, \sigma) = \begin{bmatrix} c_\phi c_\theta c_{\sigma-\phi} - s_\phi s_{\sigma-\phi} & -c_\phi c_\theta s_{\sigma-\phi} - s_\phi c_{\sigma-\phi} & c_\phi s_\theta \\ s_\phi c_\theta c_{\sigma-\phi} + c_\phi s_{\sigma-\phi} & -s_\phi c_\theta s_{\sigma-\phi} + c_\phi c_{\sigma-\phi} & s_\phi s_\theta \\ -s_\theta c_{\sigma-\phi} & s_\theta s_{\sigma-\phi} & c_\theta \end{bmatrix} \quad (1)$$

where $c_\phi = \cos \phi$, $s_\phi = \sin \phi$, $c_\theta = \cos \theta$, $s_\theta = \sin \theta$, $c_{\sigma-\phi} = \cos(\sigma - \phi)$, and $s_{\sigma-\phi} = \sin(\sigma - \phi)$.

Observing the above-rotation matrix, many will argue that these so-called T&T angles are in fact ZYZ Euler angles, where the spin angle *ψ* has been replaced with *σ* - *φ*. To some extent, this is true. So, one can think of T&T angles as a slight modification of ZYZ Euler angles. This modification is not absolutely necessary but it leads to significant simplifications.

One of the properties of any three-angle orientation representation is that a given orientation can be represented by at least two triplets of angles. In our case, the triplets {*φ*, *θ*, *σ*} and {*φ* ± 180°, -*θ*, *σ*} are equivalent. To avoid this and the representational singularity at *θ* = 180° (which is hardly achieved by any parallel robot), we set the ranges of the azimuth, tilt, and torsion as, respectively, $\phi \in (-180^\circ, 180^\circ)$, $\theta \in [0, 180^\circ)$ and $\sigma \in (-180^\circ, 180^\circ]$.

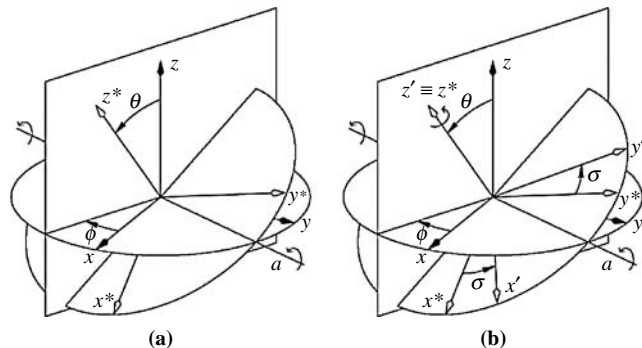
2.2 Nominal hexapod’s geometry

Before computing the workspace, we need to define the geometric parameters of the mechanism. Let us denote as *A_i* (in the following of this paper, *i* = 1 to 6) the passive joint centres of the Cardan joints attached to the base corresponding to actuator *i*, and as *B_i* the passive joint centres of the Cardan joints attached to the moving platform. All joint centres *A_i* (resp. *B_i*), are located in a plane. The origin of the base frame *R_B*, is located at the barycentre of all points *A_i*, and the origin of the moving platform frame *R_{PL}* is at point *P*, the barycentre of all points *B_i*. The positions of points *A_i* (resp. *B_i*) with respect to the origin *O* (resp. *P*) are given in Table I. Moreover, the displacements of the actuators are comprised between $|A_i B_i| = 1,143$ and $|A_i B_i| = 1,651$ mm. All this information can be found in the manufacturer’s specifications of the hexapod.

Table I Nominal coordinates of the joint centres

Joint	Coordinates along		
	x-Axis (mm)	y-Axis (mm)	z-Axis (mm)
<i>A</i> ₁	-1,066.8	127	0
<i>A</i> ₂	423.418	987.298	0
<i>A</i> ₃	643.382	860.298	0
<i>A</i> ₄	643.382	-860.298	0
<i>A</i> ₅	423.418	-987.298	0
<i>A</i> ₆	-1,066.8	-127	0
<i>B</i> ₁	516.382	640.334	0
<i>B</i> ₂	-296.418	767.334	0
<i>B</i> ₃	812.8	127	0
<i>B</i> ₄	812.8	-127	0
<i>B</i> ₅	-296.418	-767.334	0
<i>B</i> ₆	516.382	-640.334	0

Figure 2 The successive rotations of the T&T angles



Notes: (a) Tilt and (b) torsion

2.3 Constant-orientation workspace in CATIA

Many parameters influence the size of the workspace of a parallel robot. Among the main ones, we can mention:

- ranges of the joints (passive or active);
- shapes of the base and mobile platform;
- mechanical interferences; and
- singular configurations.

Several methods can be used in order to find the shape of the workspace of a manipulator (Merlet, 2006). As numerical methods give only an approximation of the shape of the workspace, which depends on the discretization step, it is preferable to use geometrical approaches which will give the exact form of the workspace. However, such methods are difficult to program as standalone programs and do not allow the creation of a good-quality representation. For this reason, it has been proposed in Bonev and Ryu (2001) to use computer-aided design (CAD) software such as CATIA to draw the shape of a workspace.

As explained in Merlet (2006), the constant orientation workspace can be found as the intersection of six so-called vertex spaces. Analyzing the vertex space of a leg, and assuming that the only limitation is the stroke of the linear actuators, it may be represented by a hollow sphere, or a half hollow sphere, if we only consider the portion superior to the plane of the base (Figure 3). Thus, the constant-orientation workspace, for a given orientation of the mobile platform, is obtained by the intersection of the six vertex spaces, which can easily be programmed in CATIA (Figure 4).

Figure 3 Vertex space of a leg – CAD representation

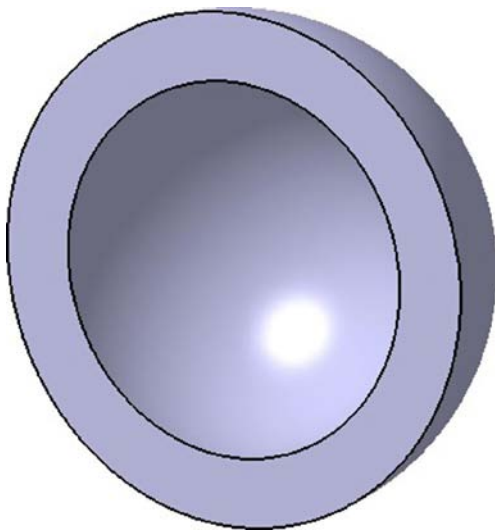
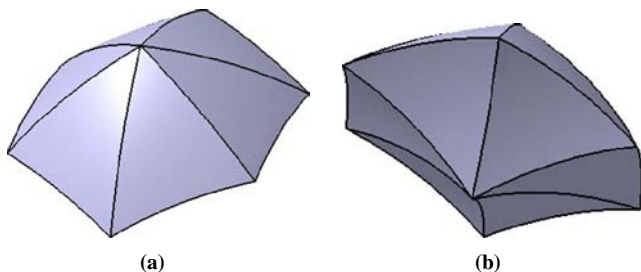


Figure 4 Intersection of the 6 vertex spaces for a given orientation of the platform



Notes: (a) Top view and (b) bottom view

2.4 Maximum tilt workspace in CATIA

The maximum tilt workspace may be defined as the total reachable volume, for any angle ϕ of the mobile platform for a given maximum tilt angle θ_{\max} . In other words, the maximum tilt workspace is the set of all positions that the centre of the mobile platform can attain, with any tilt angle between 0 and θ_{\max} , and any azimuth (any angle ϕ). Therefore, this workspace may be found as the intersection of all constant-orientation workspaces for any angle i , and any tilt angle θ between 0 and θ_{\max} , and any angle ϕ between -180° and 180° . In Bonev and Ryu (1999), it was shown through examples that for a given azimuth (ϕ) and tilt angle (θ), the workspace is nearly largest for $\sigma = 0$. Therefore, we can approximate the maximum tilt workspace as the intersection of all constant-orientation workspaces for any angle ϕ , any tilt angle θ between 0 and θ_{\max} , and $\sigma = 0$.

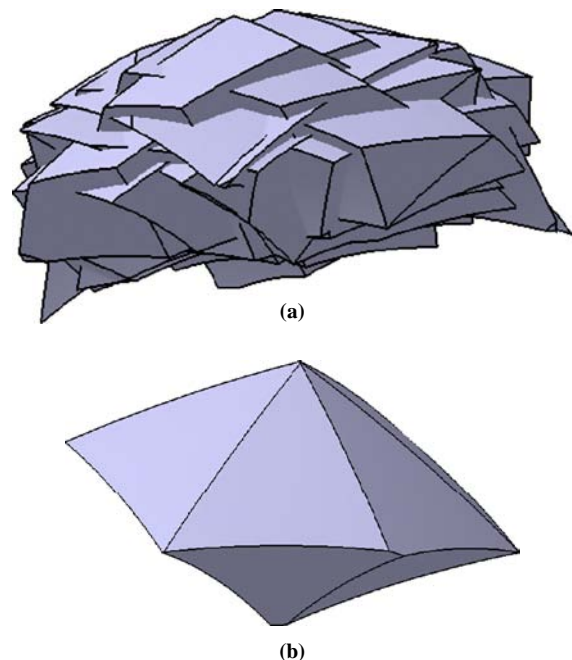
Of course, there is no analytic method for finding this workspace, so we would rather use some discretization here. First of all, we have to fix the value of the maximal tilt angle θ for which the workspace should be defined. Then, for several discrete values of ϕ and θ in the studied orientation intervals ($\phi \in (-180^\circ, 180^\circ]$, $\theta \in [0^\circ, \theta_{\max}]$), we plot all constant-orientation workspaces of the robot (Figure 5(a)). Finally, using CATIA, we intersect all these volumes in order to obtain the maximal tilt workspace (Figure 5(b)).

Note that the result is an approximation but the good thing is that all points from this approximation are inside the actual maximum tilt workspace. In other words, we claim that the maximum tilt workspace is at least the one that we can obtain with our method. Also, note that it takes about several seconds to obtain the approximation shown in Figure 5(b).

2.5 Inscribed spheres and cylinders

Obviously, the previously presented representations of the maximum tilt workspace are inadequate for an industrial use of robots, because the shape is still too much complex

Figure 5 (a) All constant-orientation workspaces of which the intersection gives and (b) the maximal tilt workspace



to analyze. Therefore, it is preferable to define a workspace with a simpler form inscribed in the maximum tilt workspace, such as a sphere or a cylinder.

2.5.1 Maximal inscribed spheres

The problem remains to find the radius and the position of the centre of the largest possible sphere inscribed in the workspace (Figure 6). Such a problem cannot be solved analytically. Therefore, we propose to treat it numerically.

First, we chose the coordinates of the centre of gravity of the analyzed volume as the departure point. We define a vertical line L passing through this point. For any point Q along this line, we will create a sphere S centered in Q of an arbitrary radius r . Then, using CATIA, we make the intersection between S and the analyzed workspace. We compare the volume of S and of the intersection. If these volumes are equal, so the sphere is inscribed in the workspace and we enlarge the radius r ; if not, the radius of the sphere is larger and we decrease it. Thus, incrementally, it is possible to find the largest radius of the sphere centred in Q and inscribed in the workspace, and retain it. Doing it for any point Q of the vertical line, and comparing all maximal radii, we can find the maximal inscribed sphere (Figure 6).

The results, for the Stewart-Gough platform under study are shown in Figure 7. It is interesting to note that the radius of the maximal inscribed sphere is linearly proportional to the tilt angle and its center is almost constant.

2.5.2 Maximal inscribed cylinders

Defining the maximal inscribed cylinder is a more complicated task, because a cylinder, contrary to a sphere, is defined by two parameters: its radius and its height. However, the task globally remains the same: finding the cylinder inscribed in the workspace, which has the greatest volume (Figure 8).

To find this cylinder, we propose to proceed as follows. For a point Q belonging to the vertical axis L , we first fix a small

Figure 6 Maximal inscribed sphere

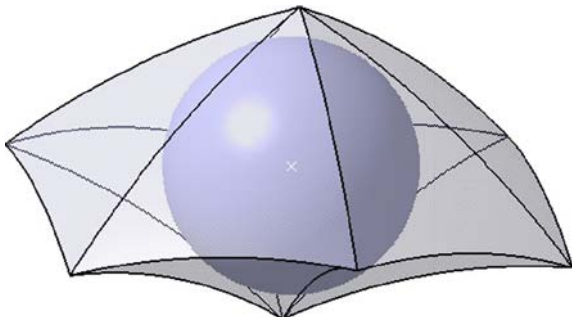


Figure 7 Maximal inscribed spheres in the maximal tilt workspaces

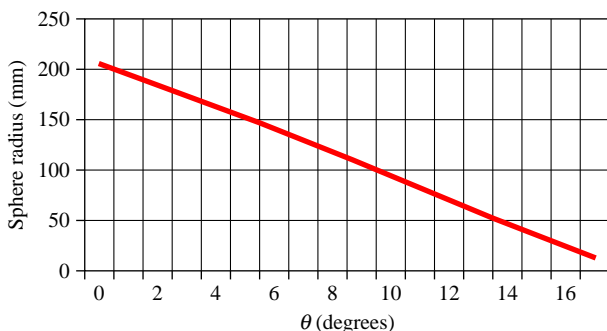
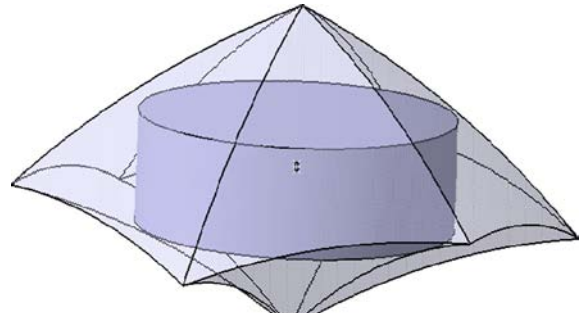


Figure 8 Maximal inscribed cylinder



radius of the cylinder and find the maximal admissible height, which allows the cylinder C to be inscribed in the workspace (following a procedure equivalent to that used in the case of the sphere). We retain the volume of this cylinder and run this algorithm again for a larger value of the radius, until we find the cylinder with the maximal volume. Once it is found, then we apply this procedure once more for another point of the axis L . Doing it for any point Q of the vertical line L , and comparing all maximal volumes, we can find the maximal inscribed cylinder (Figure 8).

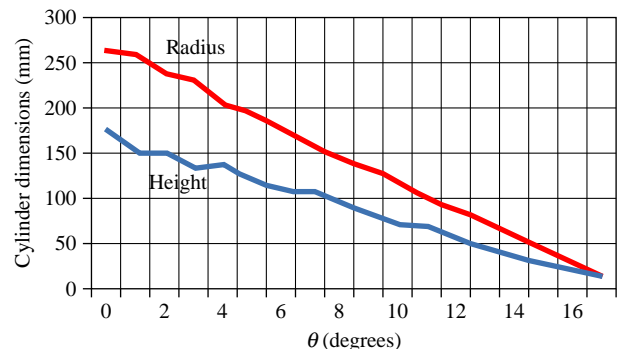
The results, for the Stewart-Gough platform under study are shown in Figure 9. It is interesting to note that, once again, the radius and the height of the maximal inscribed cylinder are almost linearly proportional to the tilt angle and its center is nearly constant for any tilt angle.

2.5.3 Singularities

Now that the workspace of the manipulator is defined, the most important step is to verify that there are no singularities in it. Analyzing the singularities of a hexapod is not a simple task and is still an open problem (Li *et al.*, 2006, 2007; Merlet, 2006; St-Onge and Gosselin, 2000). Singularities can be divided into the two main groups:

- 1 Serial singularities for which the manipulator loses one (or more) DOF. For the hexapod, they only appear if the length of one actuator is null, which is impossible from a practical standpoint.
- 2 Parallel singularities for which the manipulator gains at least one DOF. A parallel robot cannot cross such singularities (unless some complex tricks are performed, such as using gravity or inertia) and can even break up in their vicinity. The problem is that near such singularities, the motors are required to exert huge forces or torques.

Figure 9 Maximal inscribed cylinders in the maximal tilt workspaces



It is very difficult to analyse the singularities of a hexapod analytically, therefore a numerical method is preferred. The first step is to discretize the workspace of the robot, and for each point at a given orientation, to look at the sign of the determinant of the Jacobian matrix. If between two discrete points, the sign changes, we have crossed a singular configuration. Of course, the accuracy of these results depends on the step used in the discretization. But for rather small steps, there are few chances that the program does not detect a singularity.

So, we ran such an algorithm using Matlab for a wide range of constant-orientation workspaces and did not detect a singularity. Therefore, it is clear that the robot was well designed by its manufacturer.

The next part of our work will present the calibration of the hexapod.

3. Calibration

A great deal of work has been done on the calibration of parallel robots (Andreff *et al.*, 2004; Chai *et al.*, 2002; Daney, 2003), but, owing to the large variety of parallel architectures, no generalized method exists. Nearly, all these calibration methods are based on purely kinematic models (i.e. only geometrical errors are assumed). Obviously, every model is completely different from one architecture to another, but, typically, universal and spherical joints are assumed to be perfect.

Generally, the calibration of parallel robots is performed using either built-in extra sensors (Daney, 2003) or using external metrology equipment measuring (possibly only partially) the pose of the mobile platform (Andreff *et al.*, 2004; Chai *et al.*, 2002). Clearly, only the second method is suitable for calibrating an existing robot, such as our hexapod.

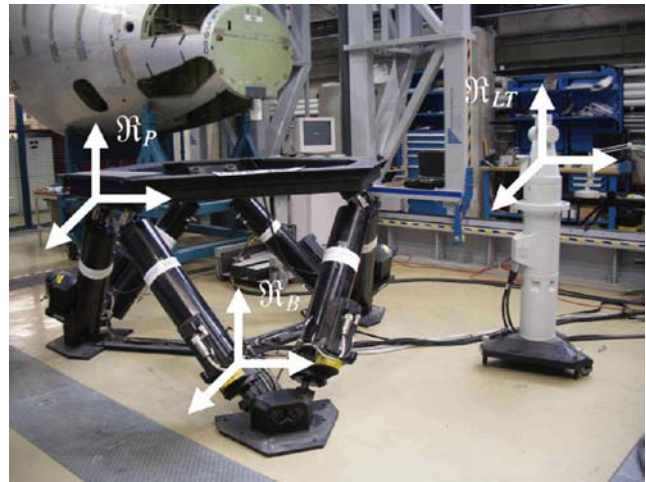
After a series of measurements has been conducted, an optimization procedure is used to estimate the set of model parameters that best approximates the output of the kinematic model to the output of the actual robot. In other words, the objective is not necessarily to correctly identify each individual parameter, but to obtain a model that best approximates the input-output relationship of the robot at the poses measured.

The vast majority of authors claim that calibration should not be time-consuming, should ideally be automated and preferably rely on low-cost measurement devices. In the aerospace context, however, (highly expensive) laser metrology systems and qualified personnel who know how to use them are currently available at all aircraft manufacturers and systems integrators for a family of applications requiring micrometer accuracy. Such applications range from the construction and certification of tooling equipment to mating and assembly of aircrafts components.

A commercial laser tracker system capable of achieving measurement accuracy of a few micrometers was available at the AMTC facility (Leica's LTD500). Naturally, our research team decided to take full advantage of this metrology equipment for the calibration of the 5000E motion platform (Figure 10).

Furthermore, since spending a few extra hours on measurements that will eventually improve the accuracy of an existing robot that costs more than a \$100,000 was not a problem, we decided to follow a completely different calibration procedure. Indeed, instead of the standard calibration approach, we measured directly each geometric characteristic of the hexapod. While this might seem to be the

Figure 10 The laser tracker calibrating the hexapod



most natural (though most time consuming) approach, there is no literature on it, let alone experimental results. While we believe that our direct approach gives better results, we made no performance comparison with the typical indirect calibration approach.

3.1 Calibration of the Cardan joints positions

The first step of our calibration method consists in finding the geometric characteristics of the hexapod, i.e. the exact positions of the centres of its Cardan joints (which are assumed to be perfect). The main principle is based on the fact that it is possible to determine the centre of a sphere, and its radius, knowing the positions of at least four (non coplanar) points located at its surface.

Thus, for finding the coordinates of the centres of the Cardan joints, it is desirable to measure the position of some points fixed on the legs for at least four configurations of the manipulator (Figure 11). These configurations have to be chosen carefully, in order to guarantee the best results. This can be done by choosing four distinct hexapod configurations (i.e. four distinct platform poses), in which a leg is displaced as far as possible in four normal directions.

Figure 11 A tooling ball fixed on the extremity of a leg



There still remains one problem: which configurations should be taken? For the base joints, by simulation, it has been found that these configurations appear for the extreme points A, B, C, D of a workspace defined by $\phi = \theta = \sigma = 0^\circ$ and $z = 307.9 \text{ mm}$ (Figure 12). For the mobile platform joints, by simulation, these configurations appear for the extreme points A, B, C, D of a workspace defined by $\phi = \theta = \sigma = 0^\circ$ and $z = 450 \text{ mm}$.

Once these points are found, the centres of the Cardan joints can be found by solving the following equation:

$$\begin{vmatrix} x^2 + y^2 + z^2 & x & y & z & 1 \\ x_A^2 + y_A^2 + z_A^2 & x_A & y_A & z_A & 1 \\ x_B^2 + y_B^2 + z_B^2 & x_B & y_B & z_B & 1 \\ x_C^2 + y_C^2 + z_C^2 & x_C & y_C & z_C & 1 \\ x_D^2 + y_D^2 + z_D^2 & x_D & y_D & z_D & 1 \end{vmatrix} = 0 \quad (2)$$

where:

x, y and z Coordinates of the joint centre.

x_Q, y_Q and z_Q Coordinates of a point Q .

It should be mentioned that, in order to have the best accuracy on the position of the joint centres, it is preferable to measure the position of more than four points, and to find the centre of joints through an optimization method. This can be done readily using any metrology software.

However, the obtained positions of the joint centres are given with respect to the laser tracker frame \mathcal{R}_{LT} which is not fixed with respect to the hexapod base, since we have to displace the laser tracker often (Figure 10). Therefore, we need to define a global reference frame \mathcal{R}_B fixed on the hexapod base that will be independent of the position of the laser tracker. In order to define the location of the reference frame \mathcal{R}_B , three reflectors are positioned on the base of the hexapod (Figure 13) and their coordinates are measured each time that the laser tracker is displaced. Another frame \mathcal{R}_P , fixed in the moving platform, is added in order to help us define the coordinates of the centres of the platform joints.

Obviously, this change of reference frames leads to a slight accumulation of errors that is different from one

Figure 12 Measurement positions for the identification of the base joint centres

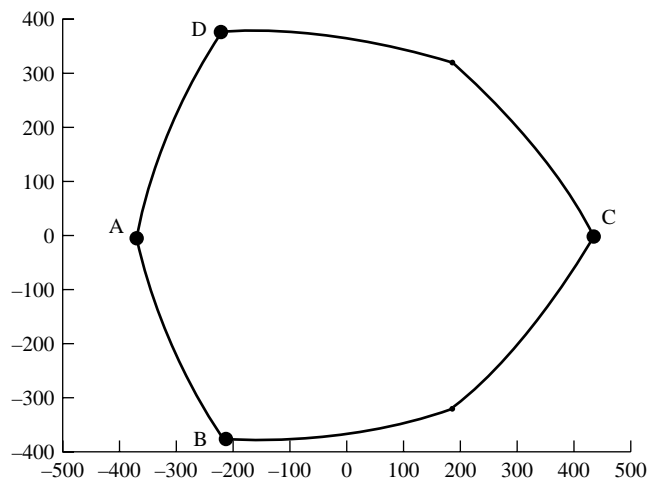
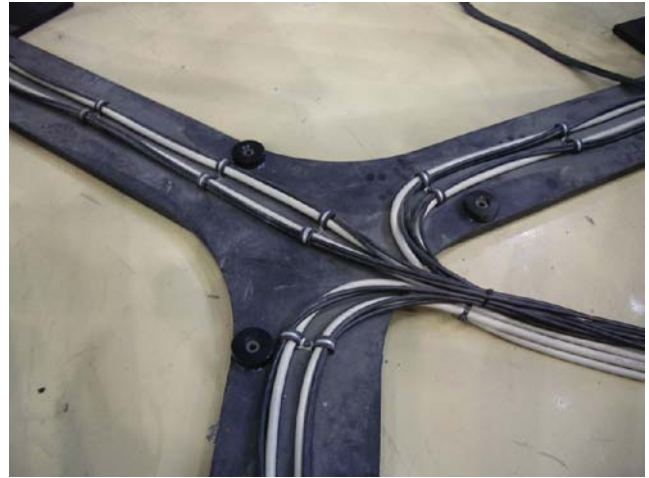


Figure 13 The three magnetic nests used for identifying the global reference frame



measurement configuration to another. However, this effect is minor compared to the large errors that we find with respect to the hexapod nominal geometry. Therefore, we do not take it into account.

Once the coordinates of the base joint centres are found, we need to fit the real base hexagon (which is non planar) to the real base hexagon, and define a new base frame. This can be done using CATIA. The first step is to define the optimal plane \mathcal{P}_{opt} that minimizes the sum of the squared distances between the real six base joint centres and the plane. Next, we can define the barycentre G of all real base joint centres. Then, using CATIA, we draw the optimal plane \mathcal{P}_{opt} (with the real position of the base joint centres) and make it coincide with the theoretical plane of the fixed base of the robot. We also make the real and nominal barycentres coincide. There still remains one free degree of rotation between the two planes: a rotation around the z -axis. In order to fix this rotation, many solutions are possible. We propose here the following approach. First, trace a point at the middle of the segment between two real base joint centres. Then, project it on the plane \mathcal{P}_{opt} and trace a line between G and this point. Make the same operation with two theoretical base joint centres, and make the two lines coincide. Thus, the last DOF is fixed.

We can follow the exact same procedure for the mobile platform. The results are presented in Tables II and III. They distances between the coordinates of the nominal and real

Table II Errors between the nominal and real values of the base joint centres

Joint	Errors			Error norm (mm)
	x-Axis (mm)	y-Axis (mm)	z-Axis (mm)	
A_1	0.279	0.158	0.465	0.565
A_2	1.327	0.969	0.071	1.645
A_3	0.381	1.032	0.36	1.157
A_4	0.834	1.264	1.79	2.345
A_5	0.699	0.736	1.711	1.989
A_6	0.308	0.158	0.254	0.429

Table III Errors between the nominal and real values of the mobile platform joint centres

Joint	Errors			
	x-Axis (mm)	y-Axis (mm)	z-Axis (mm)	Error norm (mm)
B_1	0.584	0.531	1.382	1.591
B_2	0.653	1.576	1.385	2.198
B_3	0.703	0.223	1.407	1.588
B_4	0.207	1.192	1.459	1.896
B_5	0.88	1.065	1.464	2.012
B_6	0.321	0.075	1.389	1.428

base or platform centres vary from less than 0.6 mm to more than 2.3 mm, which is significant for any positioning device.

Now that the errors on the positions of the joint centres are known, the last part of our calibration method is to define the errors on the actuators' length that are due to the control system.

3.2 Calibration of actuators' lengths

The aim of this calibration is to assess the performance of the factory control system. To perform this evaluation, the errors between the desired, or theoretical, and measured actuators' lengths are evaluated and analysed.

In order to determine these errors, we will proceed with the following approach. We enter in the control system the desired values for the actuators. Then, using the laser tracker, we can define the positions and orientations of frames \mathcal{R}_B and \mathcal{R}_P , and also the real coordinates of all 12 joint centres. Let us denote as x_{Ai} , y_{Ai} and z_{Ai} the coordinates of the base joint centre of actuator i along the x , y and z -axes, respectively, and as x_{Bi} , y_{Bi} and z_{Bi} the coordinates of the platform joint centre of actuator i along x , y and z -axes, respectively. Thus, the length ρ_i of actuator i can be found through the following relation:

$$\rho_i = \sqrt{(x_{Bi} - x_{Ai})^2 + (y_{Bi} - y_{Ai})^2 + (z_{Bi} - z_{Ai})^2} \quad (3)$$

Thus, we measure the positions of the joint centres and then compute the values of ρ_i for three configurations of the platform which correspond to the following lengths for each actuator:

- 1 8 per cent of the total actuators strut elongation;
- 2 50 per cent; and
- 3 92 per cent, i.e. 1,183.64, 1,397 and 1,610.36 mm, respectively.

The errors on the lengths are given in Table IV. They vary from 0.1 to 0.9 per cent. It will be shown next that this induces large errors to the position of the mobile platform.

3.3 Improvement of the robot accuracy

In the nominal model, since the base and the mobile platform are assumed symmetrical and, for the above three tested configurations of the robot ((1), (2), and (3)), all actuators have the same length, the position along the x - and y -axes should be equal to zero. But, as there are some errors on the positions on the joint centres and as the controller does not control precisely the length of the actuators, there are deviations from the positions along the x - and y -axes of the centre of the mobile platform and of the platform's orientation. These deviations were measured and are given in Table V. They vary from less than 0.1 mm to more than 2 mm.

Table IV Errors on the actuators' lengths

Actuator	Errors					
	Configuration (1)		Configuration (2)		Configuration (3)	
	mm	%	mm	%	mm	%
1	1.12	0.10	2.08	0.15	2.13	0.13
2	3.68	0.31	3.87	0.28	3.10	0.19
3	1.41	0.12	1.56	0.11	1.71	0.11
4	-3.06	0.26	-3.21	0.23	-3.33	0.21
5	-10.68	0.90	-10.58	0.76	-10.81	0.67
6	-7.39	0.62	-8.40	0.60	-9.69	0.61

These results clearly confirm the fact that, in addition to using a calibrated geometric model of the robot, the retrofit of the factory control system of the manipulator is also mandatory to improve the accuracy of the robot. The architecture of the controller, retrofitted using a commercial high-performance motion control platform, is briefly presented in the next section.

4. Controller retrofit

This section is provided purely for information purposes, so that this paper may also be viewed as a case study.

4.1 Requirements

As mentioned in the introduction, the motion platform acquired by the AMTC was originally designed for positioning applications involving the playback of pre-recorded trajectories. The positioning and tracking performance were well outside aerospace manufacturing precision requirements, which are in the range of 0.3 to 0.02 mm. In order to achieve this level of precision, it was found that the factory controller had both an insufficient update rate and imprecise kinematics model. Also, due to the research-oriented nature of the projects that were carried out on the platform, openness of the controller was necessary. The level of openness and reconfigurability needs to be such that different industrial applications involving this type of parallel architecture can be investigated. The requirements for the upgrade were formulated as follows:

- Cartesian path planning capability;
- full access to the kinematic model in the controller;
- CPU processing power allowing for fast controller update rates;
- control of actuator torques;
- user interface allowing for online monitoring and data acquisition;
- access to controller gains;
- possibility of performing model-based control; and
- data acquisition and monitoring of control signals.

As the original power supply and amplification system was deemed capable of meeting the requirements, the controller retrofit had to interface with the existing electrical layout.

4.2 New controller configuration and features

The original configuration comprised of an industrial PC hosting the controller running under DOS, responsible for sending out joint-level commands. A programmable logic controller (PLC) was also present to provide braking, security and other

Table V Errors on the position of the reflectors of the mobile platform

Reflector	Configuration (1)		Errors		Configuration (3)	
	x-Axis (mm)	y-Axis (mm)	x-Axis (mm)	y-Axis (mm)	x-Axis (mm)	y-Axis (mm)
1	-0.069	-0.358	-0.707	-1.162	-1.645	-2.197
2	-0.199	-1.162	-0.814	-1.104	-1.696	-2.229
3	-0.2	-2.197	-0.81	-1.138	-1.78	-2.241

supervisory functions. Command signals were acquired and sent to the motor drives through a custom-made interface board. Access to the controller via the graphical interface was done using a standard screen and keyboard configuration.

The main component of the new controller architecture is a Delta Tau Universal Motion and Automation Controller system. The system incorporates a digital signal processor-based motion controller capable of handling up to 32 axes as well as the analog and digital inputs/outputs required to control and monitor the system, thereby fulfilling the role of the old control computer and PLC combined. The communication channels directly interface with the motor drives, from which resolver signals are read and resulting commands sent to. Figure 14 shows the system architecture before and after the controller upgrade.

The motion controller holds all the necessary algorithms to perform advanced monitoring and control functions. Some of the features of the motion controller are as follows:

- trajectories programmable using linear interpolation, circular interpolation or B-splines;
- Cartesian-level path-planning via user-programmable inverse kinematics;
- self-tunable proportional integral derivative loops with variable gains;

- S-curve acceleration profile;
- ability to include look-up tables; and
- look-ahead filter based on velocity and acceleration limitations on the trajectory.

The user interface, as shown in Figure 15, was programmed in Visual Basic and allows for real-time monitoring and data acquisition of controller signals. The kinematic parameters resulting from the above-described calibration procedure were included in the model used by the motion controller. Also, Cartesian workspace limitations as a function of platform orientation were also implemented for path-planning considerations.

5. Conclusions

This paper is the result of a collaborative research project aimed at converting a popular commercial motion base to an industrial robot for use in heavy duty aerospace manufacturing processes. A kinematic analysis of the workspace characteristics showed that the conventional octahedral hexapod design has a very limited workspace, though free of singularities. A novel 3D measure of workspace and a simple method for its computation were presented.

Figure 14 Schematic of the factory controller retrofit

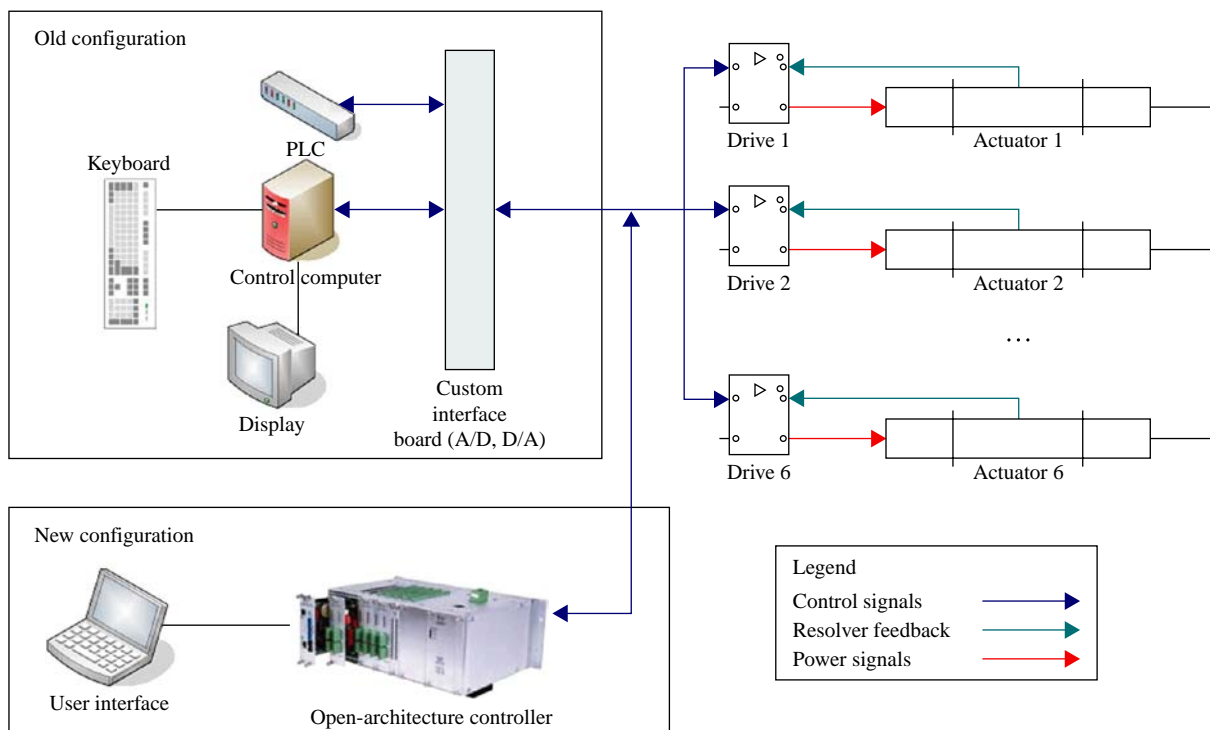
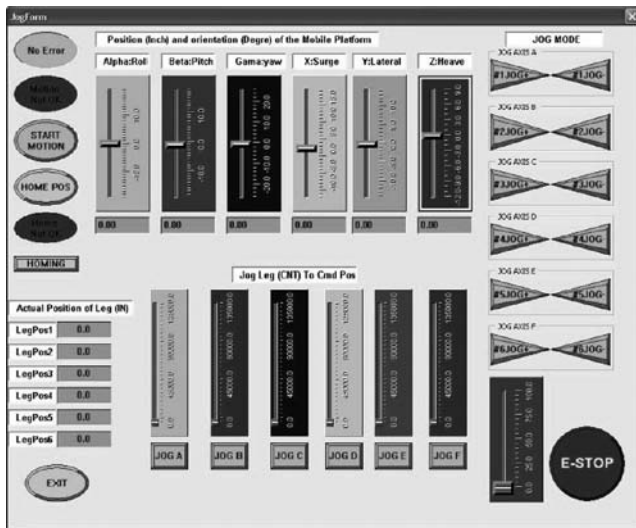


Figure 15 User interface for manual jogging mode



In addition, a simple and intuitive calibration procedure was proposed for directly measuring the geometry of the hexapod using a laser tracker. It was shown that important deviations exist between the actual and the factory kinematic models. Finally, we presented some information regarding the retrofit of the existing hexapod controller using a high performance off-the-shelf motion controller incorporating the previously determined workspace characteristics and calibration data. Upcoming work includes system performance benchmarks in positioning precision.

References

- Andreff, N., Renaud, P., Martinet, P. and Pierrot, F. (2004), "Vision-based kinematic calibration of an H4 parallel mechanism: practical accuracies", *Industrial Robot*, Vol. 31 No. 3, pp. 273-83.
- Bonev, I.A. (2003), "The true origins of parallel robots", *ParalleMIC*, January, available at: www.parallemic.org/Reviews/Review007.html (online review).
- Bonev, I.A. and Ryu, J. (1999), "Orientation workspace analysis of 6-DOF parallel manipulators", *Proceedings of the ASME Design Engineering Technical Conferences (DETC 1999)*, Las Vegas, NV, USA, 12-15 September.
- Bonev, I.A. and Ryu, J. (2001), "A geometrical method for computing the constant-orientation workspace of 6-PRRS parallel manipulators", *Mechanism and Machine Theory*, Vol. 36 No. 1, pp. 1-13.
- Bonev, I.A., Zlatanov, D. and Gosselin, C.M. (2002), "Advantages of the modified Euler angles in the design and control of PKMs", *Proceedings of the 2002 Parallel Kinematic Machines International Conference, Chemnitz, Germany, 23-25 April*, pp. 171-88.
- Chai, K.-S., Young, K. and Tiersley, I. (2002), "A practical calibration process using partial information for a commercial Stewart platform", *Robotica*, Vol. 20, pp. 315-22.
- Collado, V. and Herranz, S. (2004), "Space 5H: a new machine concept for 5-axis milling of aeronautics structural

components", *Proceedings of the 4th Chemnitz Parallel Kinematics Seminar*, pp. 611-24.

- Crawford, N.R., Yamaguchi, G.T. and Dickman, C.A. (1999), "A new technique for determining 3-D joint angles: the tilt/twist method", *Clinical Biomechanics*, Vol. 14 No. 3, pp. 153-65.
- Daney, D. (2003), "Kinematic calibration of the Gough platform", *Robotica*, Vol. 21, pp. 677-90.
- Hennes, N. and Staimer, D. (2004), "Application of PKM in aerospace manufacturing-high performance machining centres ECOSPEED, ECOSPEED-F and ECOLINER", *Proceedings of the 4th Chemnitz Parallel Kinematics Seminar*, pp. 557-68.
- Hennessey, C.W. (2004), "Parallel kinematic micromanipulator", US Patent No. 6,769,194, Alexandria, VA.
- Huang, T., Wang, J. and Whitehouse, D.J. (1999), "Closed form solution to workspace of hexapod-based virtual axis machine tools", *Journal of Mechanical Design*, Vol. 121, pp. 26-31.
- Kihlman, H. and Engström, M. (2002), "Affordable reconfigurable tooling", *Transactions of the Journal of Aerospace*, Vol. 18 No. 4, pp. 463-74.
- Kihlman, H., Ossbahr, G., Engström, M. and Anderson, J. (2004), "Low-cost automation for aircraft assembly", *Proceedings of the Aerospace Manufacturing and Automated Fastening Conference, St Louis, MO*, pp. 117-24.
- Korein, J.U. (1984), *A Geometric Investigation of Reach*, MIT Press, Cambridge, MA.
- Li, H., Gosselin, C.M. and Richard, M.J. (2007), "Determination of the maximal singularity-free zones in the six-dimensional workspace of the general Gough-Stewart platform", *Mechanism and Machine Theory*, Vol. 42 No. 4, pp. 497-511.
- Li, H., Gosselin, C.M., Richard, M.J. and Saint-Onge, B.M. (2006), "Analytic form of the six-dimensional singularity locus of the general Gough-Stewart platform", *Journal of Mechanical Design*, Vol. 128 No. 1, pp. 279-87.
- Merlet, J.-P. (2006), *Parallel Robots*, 2nd ed., Springer, New York, NY.
- Sàenz, A.J., Collado, V., Giménez, M. and Sebastian, I. (2002), "New automation solutions in aeronautics through parallel kinematic systems", *Proceedings of the 3rd Chemnitz Parallel Kinematics Seminar*, pp. 563-78.
- St-Onge, B.M. and Gosselin, C.M. (2000), "Singularity analysis and representation of the general Gough-Stewart platform", *The International Journal of Robotics Research*, Vol. 19 No. 3, pp. 271-88.
- Wang, Y. (1999), "Workspace analysis of a novel closed-chain manipulator", PhD thesis, Case Western Reserve University, Cleveland, OH.

Further reading

- Gosselin, C.M. and Angeles, J. (1990), "Singularity analysis of closed-loop kinematic chains", *IEEE Transactions on Robotics and Automatics*, Vol. 6 No. 3, pp. 281-90.

Corresponding author

Ilian Bonev can be contacted at: ilian.bonev@etsmtl.ca